The gas–liquid phase-transition singularities in the framework of the liquid-state integral equation formalism

Gari Sarkisov
Institute of Theoretical and Experimental Biophysics, Russian Academy of Sciences, 142290 Pushchino, Moscow Region, Russia

Enrique Lomba[a)]
Instituto de Química Física Rocasolano, Consejo Superior de Investigaciones Cientificas (CSIC)/Serrano 119, E-28006 Madrid, Spain

(Received 23 March 2005; accepted 7 April 2005; published online 2 June 2005)

The singularities of various liquid-state integral equations derived from the Ornstein–Zernike relation and its temperature derivatives, have been investigated in the liquid–vapor transition region. As a general feature, it has been found that the existence of a nonsolution curve on the vapor side of the phase diagram, on which both the direct and the total correlation functions become complex—with a finite isothermal compressibility—also corresponds to the locus of points where the constant-volume heat capacity diverges, in consonance with a divergence of the temperature derivative of the correlation functions. In contrast, on the liquid side of the phase diagram one finds that a true spinodal (a curve of diverging isothermal compressibilities) is reproduced by the Percus–Yevick and Martynov–Sarkisov integral equations, but now this curve corresponds to states with finite heat capacity. On the other hand, the hypernetted chain approximation exhibits a nonsolution curve with finite compressibilities and heat capacities in which, as temperature is lowered, the former tends to diverge. © *2005 American Institute of Physics*. [DOI: 10.1063/1.1925269]

I. INTRODUCTION

In a preliminary investigation[1] the authors presented an analysis of the vapor–liquid transition singularities based both on the behavior of approximate Ornstein–Zernike integral (OZ) equations and the appropriate integral equations for the temperature derivatives of correlation functions. With this set of equations, along with the regular thermodynamic functions such as energy, isothermal compressibility, and compressibility factor, which are calculated through the radial correlation function, it is possible to evaluate directly the constant-volume heat capacity in terms of the temperature derivative of the thermal potential. This makes feasible the study of the transition singularities just related to the heat capacity.

It is a well-known fact that in a great number of cases, approximate OZ equations in systems that undergo phase separations present a locus of nonsolution points, which does not coincide neither with the phase-equilibrium curve (binodal) nor with the thermodynamic instability curve (spinodal), this nonsolution line being located somewhere between binodal and spinodal in the vapor side of the phase diagram.[2–5] Interestingly, the hypernetted chain (HNC) approximation presents also the same features on the liquid side of the phase diagram. What is really noteworthy is that all thermodynamic quantities that can be directly calculated from the radial correlation function, such as isothermal compressibility, energy, and pressure, remain finite in the vicinity of the nonsolution curve and thus, even if one can say that the singularity in the equation is a signature of a phase transition, its true physical nature remains somewhat unclear. On the other hand, from the mathematical point of view, in Refs. 3–5 it was unambiguously shown that the lack of solution is due to the presence of square-root branch points (SRBP) that signal the onset of complex solutions. In Ref. 3 it was also shown that on the liquid side of the phase diagram at sufficiently low temperatures, the HNC equation seems to hit a true spinodal when lowering the density along an isotherm, and the solutions obtained in the thermodynamically unstable domain present poles for nonzero k values (k being the reciprocal space vector) in the complex plane associated with a long-ranged oscillatory behavior. A similar type of behavior was characterized by Root and Lovett[6] in their solution of the Yvon–Born–Green equation for the one-dimensional Gaussian core model, and it was interpreted as an indication of the presence of inhomogeneities. Whether this is exactly the case we have at hand, remains open for discussion.

Now for the Percus–Yevick (PY) approximation, the analytic study carried out on the adhesive hard-sphere fluid by Cummings and Stell[7] showed that on the vapor side the PY equation yields a nonsolution curve corresponding to SRBPs, whereas on the liquid side a true spinodal is found, both curves meeting at the critical point. This a situation somewhat more definite than the one mentioned above for the HNC, where the transition from one type of behavior to the other takes place smoothly on the liquid side of the phase diagram as temperature is lowered, and not in a certain point of particular physical significance.

Another class of behavior worth mentioning is that of the mean spherical approximation (MSA). This simple linearized approximation always reproduces the presence of a

[a)]Electronic mail: e.lomba@iqfr.csic.es

true spinodal, as was shown by Cummings and Monson[8] for the attractive hard-core Yukawa fluid. Interestingly, this type of approximation at low density and low temperature is known to perform poorly when compared with PY or HNC for the simple reason that it does not even preserve the second virial coefficient, and thus cannot account for pairing effects, which are essential at low temperatures at the onset of condensation. Thus the fact that the MSA renders true spinodals cannot certainly be considered a virtue of the approximation.

In any case, what we do know is that approximations that are known to be good in the low-density regime, such as HNC or PY, do present a somewhat unphysical feature soon after the binodal line is transversed along an isotherm—in the rather extreme case of electrolytes even before the binodal is reached.[5] On the other hand, it is also important to note that no qualitative differences between correlation functions in the stable (outside the binodal) and metastable (inside the binodal and outside the spinodal) regions are observed. However, if we take into account the exact statistical mechanical definitions, then according to the Van Hove theorem,[9] the limit of the single-phase stable states of a spatially uniform system is, the phase equilibrium line, that is, the binodal, on which the derivatives of the thermodynamic potential have discontinuities. This condition applies to the thermodynamic limit, i.e., $N\to\infty$, $V\to\infty$, with a constant number density $\rho=N/V$. Note that in the thermodynamic limit the theory applies neither to metastable states nor to spinodals. We could therefore expect that the solutions to the exact OZ equations, which are considered equivalent to the Gibbs distribution in the thermodynamic limit, should disappear or exhibit singularities on the phase equilibrium boundaries. Nonetheless, this is not the case. It is then the situation that we can use the solutions obtained in the metastable regime and somehow expect that the mathematics of the integral equation mimic nature and produce results that can be comparable to the experiment on the metastable region. With a few exceptions, this is indeed what happens, but no convincing theoretical explanation is at hand to clarify why it is so. Nonetheless, when working in the metastable regime one must be cautious since the presence of multiple solutions[3,4] implies that some of them lack any physical significance and must be discarded.

In this work we intend to shed some light onto this rather confusing situation. To that purpose we have here focused on three well-established integral equation approximations, the HNC, PY, and the Martynov–Sarkisov (MS) closure[2] for which we have analyzed the solutions (both real and complex) in the neighborhood of the vapor–liquid transition for a classical Lennard-Jones (LJ) fluid. In parallel with the solution of this integral equations we have also solved the corresponding equations for the temperature derivatives of the OZ relation plus HNC, PY, and MS closures. As mentioned before, this enables a direct evaluation of the constant-volume heat capacity the singularities of which will also be analyzed. The rest of the paper is organized as follows. In Sec. II we summarize all equations and central aspects of the theory, which we use in our calculations. Results and discussions are presented in Sec. III.

II. BASIC EQUATIONS AND FORMULAS

An essential part of our analysis focuses on the behavior of the constant-volume heat capacity, which, in a system with pairwise additive interactions, is defined by

$$C_\nu=(\partial E/\partial T)_\nu=(\partial E/\partial T)_\rho=\tfrac{3}{2}k_BN+2\pi N\rho\int\Phi(r)\times(\partial g(r)/\partial T)_\rho r^2dr, \tag{1}$$

where N is the particle number, k_B is Boltzmann's constant, $g(r)$ is the pair distribution function, and Φ is the interaction potential. In Eq. (1) the standard definition for internal energy

$$E=\tfrac{3}{2}k_BNT+2\pi N\rho\int\Phi(r)g(r)r^2dr \tag{2}$$

is implicit. As mentioned in the Introduction, herein we will deal with fluids composed of particles interacting via the Lennard-Jones potential

$$\Phi(r)=4\varepsilon\left[\left(\frac{\sigma}{r}\right)^{12}-\left(\frac{\sigma}{r}\right)^{6}\right],$$

where ε measures the well depth of the potential and σ is the range parameter. As usual we will define a reduced temperature as $T^*=k_BT/\varepsilon$.

The radial correlation function relates to the interaction potential through

$$g(r)=\exp(-\beta\Phi(r)+\omega(r)), \tag{3}$$

with $\beta=1/k_BT$ as usual, and the thermal potential $\omega(r)$ being defined by

$$\omega(r)=\gamma(r)+B(r)=h(r)-C(r)+B(r). \tag{4}$$

Here $h(r)=g(r)-1$ is the total correlation function, $C(r)$ is the direct correlation function, and $B(r)$ is the bridge functional, which can be defined in terms of an infinite series of irreducible diagrams. Differentiating (3) one gets

$$(\partial g(r)/\partial T)_\rho=\frac{g(r)}{T}[\beta\Phi(r)+T(\partial\omega(r)/\partial T)_\rho] \tag{5}$$

by which we then obtain for the reduced excess heat capacity

$$C_\nu^*=\frac{C_\nu}{Nk_B}-\frac{3}{2}=2\pi\rho\int\beta\Phi(r)g(r)[\beta\Phi(r)-\beta(\partial\omega(r)/\partial\beta)_\rho]r^2dr. \tag{6}$$

It follows that in addition to the radial correlation function $g(r)$, we should know the function $Y(r)=-\beta(\partial\omega(r)/\partial\beta)_\rho$ to calculate the heat capacity. The equation for $Y(r)$ can be directly derived from the OZ equation

$$h(r_{12})=C(r_{12})+\rho\int C(r_{13})h(r_{23})d\mathbf{r}_3 \tag{7}$$

and the closure relation. In the HNC approximation $g(r)$ and $Y(r)$ are determined by means of Eq. (7) together with $B=0$, i.e., $\omega=\gamma$, by which one gets

$$\omega(r_{12})=\rho\int[h(r_{13})-\omega(r_{13})]h(r_{23})d\mathbf{r}_3, \tag{8}$$

$$Y(r_{12}) = \rho \int [g(r_{13})\beta\Phi(r_{13}) + h(r_{13})Y(r_{13})]h(r_{23})d\mathbf{r}_3 + \rho \int C(r_{13})g(r_{23})[\beta\Phi(r_{23}) + Y(r_{23})]d\mathbf{r}_3. \quad (9)$$

In the PY approximation the bridge function can be written as

$$B(r) = \log(1 + \gamma(r)) - \gamma(r) = 1 + \omega(r) - \exp\omega(r), \qquad \gamma(r) = e^{\omega(r)} - 1, \quad (10)$$

and

$$\exp\omega(r_{12}) - 1 = \rho \int (f(r_{13}) - 1)\exp\omega(r_{13})h(r_{23})d\mathbf{r}_3, \quad (11)$$

$$Y(r_{12})[1 + \gamma(r_{12})] = \rho \int [g(r_{13})\beta\Phi(r_{13}) + C(r_{13})Y(r_{13})]h(r_{23})d\mathbf{r}_3 + \rho \int C(r_{13})g(r_{23})(\beta\Phi(r_{23}) + Y(r_{23}))d\mathbf{r}_3, \quad (12)$$

where f is the Mayer function $f(r)=\exp(-\beta\Phi(r))-1$.

Finally, the Martynov–Sarkisov closure[10] reads

$$B(r) = -\tfrac{1}{2}\omega(r)^2 = \sqrt{1 + 2\gamma(r)} - \gamma(r) - 1. \quad (13)$$

This approximation has proven to be fairly accurate and thermodynamically consistent for hard-sphere fluids and must be modified along the lines suggested by Duh and co-workers[11] in order to extend its range of applicability to attractive potentials, such as the Lennard-Jones interaction.[2] Thus, here we will have

$$B(r) = -\tfrac{1}{2}\Omega(r)^2 = \sqrt{1 + 2s(r)} - s(r) - 1, \quad (14)$$

where $\Omega(r)=\omega(r)-\rho\beta\Phi(r)_{\text{att}}$ and $s(r)=\gamma(r)-\rho\beta\Phi_{\text{att}}(r)$. Φ_{att} is the term in the interparticle interaction potential responsible for the dispersive forces (attractive interactions). It is customary to take this term as the perturbation part in a Weeks–Chandler–Anderson (WCA) division of the interaction potential.[12] This approximation has proven to be valid up to the melting line along which $s(r)=-0.5$ and $\Omega(r)=-1$. To extend its solutions inside the crystallization area (amorphous states) the closure (14) has been modified as follows[2]

$$B(r) = \text{sign}(\sqrt{|1 + 2s(r)|}) - s(r) - 1, \quad (15)$$

where "sign" means the sign of $(1+2s(r))$.

The OZ equation with the closure (15) covers both the vapor–liquid stable and metastable region, in addition to those metastable liquid states that arise in the liquid–solid transition region. Thus we have finally

$$\omega(r_{12}) + \tfrac{1}{2}\Omega(r_{12})^2 = \rho \int \left[h(r_{13}) - \omega(r_{13}) - \tfrac{1}{2}\Omega(r_{13})^2\right]h(r_{23})d\mathbf{r}_3, \quad (16)$$

$$Y(r_{12})[1 + \Omega(r_{12})] = \rho \int [g(r_{13})\beta\Phi(r_{13}) + (h(r_{13}) - \Omega(r_{13}))Y(r_{13})]h(r_{23})d\mathbf{r}_3 + \rho \int C(r_{13})g(r_{23})(\beta\Phi(r_{23}) + Y(r_{23}))d\mathbf{r}_3. \quad (17)$$

Provided a solution for $g(r)$ to the OZ equation exists, solving corresponding equations for $\omega(r)$ derivatives does not involve serious difficulties. In principle they can be found using direct iterations, however, once we enter the space of complex solutions it is advisable to use a more sophisticated approach like the one proposed by Ng.[13] As to the solution of the OZ equation, the hybrid Newton–Raphson technique devised by Labik, Malijevsky, and Vonka[14] (LMV)—or some other similar approach—is not only efficient, but also essential in order to capture the complex solutions. The fundamentals of the method are well known and will not described here.

Finally, a few remarks deserve to be mentioned regarding the calculation of complex solutions. Following the strategy devised in Ref. 3, the OZ equation is perturbed in Fourier space with an imaginary parameter $i\epsilon$, by which Eq. (7) now reads in k space

$$\tilde{\gamma}(k) = \frac{\rho\tilde{C}(k)^2}{1 - \rho\tilde{C}(k) + i\epsilon/k}, \quad (18)$$

where the tilde denotes the Fourier transform of the original function. As in Ref. 3 the equation will be solved with its corresponding closure with a finite parameter ϵ (for instance, $\epsilon=0.001$) by which the SRBP is eliminated and the transition to the complex region is smoothed. Now once the boundary of nonsolution of the unperturbed equation is crossed, one simply lets $\epsilon\to 0$ and recovers the complex solution of the original OZ equation. The same applies to the equations for the temperature derivatives, which can be written as

$$\tilde{\gamma}'(k) = \frac{\gamma(\tilde{k}) - 2\tilde{C}(k)}{1 - \rho\tilde{C}(k) + i\epsilon/k}\rho\tilde{C}'(k), \quad (19)$$

where the primed quantities are defined by $f' = \beta\partial f/\partial\beta$.

III. RESULTS AND DISCUSSION

The calculations presented in this work have been carried out using a discretized mesh of 16 386 points with a grid size $\Delta r=0.01\sigma$. Solutions have been considered converged when the difference between the successive iterates satisfies

$$\int (\gamma^{n+1}(r) - \gamma^n(r))(\gamma^{n+1}(r) - \gamma^n(r))^* dr \approx \sum_i (\gamma^{n+1}(r_i) - \gamma^n(r_i))(\gamma^{n+1}(r_i) - \gamma^n(r_i))^* \Delta r < \xi,$$

where the asterisk denotes the complex conjugate. Here we have used $\xi=10^{-6}$.

In Fig. 1 we present the inverse of the isothermal compressibility

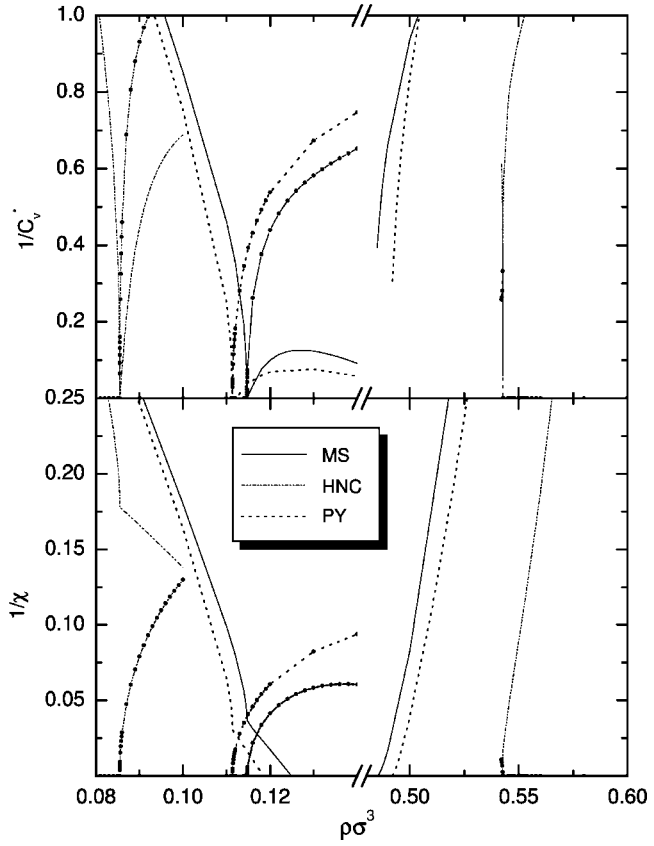

FIG. 1. Real and imaginary components (lines and lines+black circles, respectively) of the inverses of the isothermal compressibility (lower graph) and of the heat capacity (upper graph) at temperature $T^*=1.1$ for various integral equation approximations in the neighborhood of the vapor–liquid transition.

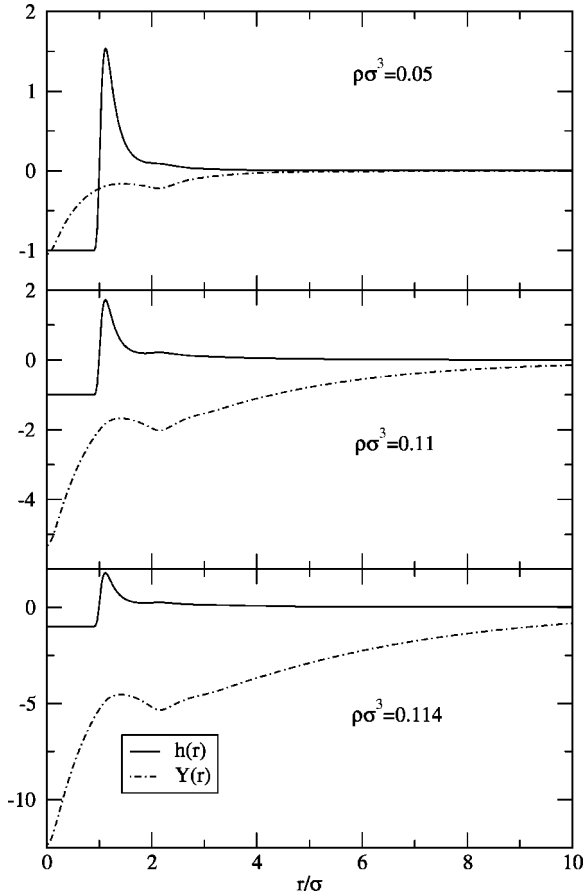

FIG. 2. Evolution of the $Y(R)$ function in the MS approximation as the density increases in the vicinity of the nonsolution boundary on the vapor side of the phase transition for the $T^*=1.1$ isotherm for MS closure. For comparison the total correlation function $h(r)$ is also shown.

$$1/\chi = (\partial\beta P/\partial\rho) = \left(1+\rho\int h(r)d\mathbf{r}\right)^{-1} = 1-\rho\int C(r)d\mathbf{r} \tag{20}$$

together with the heat capacity for all three approximations considered, at reduced temperature $T^*=kT/\varepsilon=1.1$, both on the vapor and on the liquid side of the phase diagram. Note that the critical parameters, as determined in the MS approximation[15] of Eq. (16), are $T^*_{\mathrm{cr}}=1.309$ and $\rho_{\mathrm{cr}}\sigma^3=0.29$, which are very close to computer simulation values. On the vapor side a strong divergence of C_ν is observed for all three closures when approaching the no-solution point. Actually, the solution becomes complex after crossing $1/C_\nu=0$, and in the region of complex solutions when approaching the boundary one observes that both $\mathrm{Re}\{C_\nu\}\to\infty$ and $\mathrm{Im}\{C_\nu\}\to\infty$. In order to explain this behavior let us first consider Eq. (2) for the energy. When the distance r tends to infinity, the potential $\Phi(r)$ goes to zero as $1/r^6$, and the radial correlation function $g(r)$ is finite everywhere. The energy is therefore also finite everywhere, including right at the critical point. According to (6), the heat capacity is always finite if $Y(r)$ is finite. It follows that the singular behavior of the heat capacity can only be related to the growth of the $Y(r)$ function itself. As the $Y(r)$ function is continuous, this occurs over a whole range of r values. This conclusion is strongly supported by Fig. 2, where the evolution of $Y(r)$ with density when approaching the singularity is depicted. At the same time the reduced compressibility has no tendency to grow significantly when approaching the nonsolution locus. This is also determined by the structure of $g(r)$ (see Fig. 2). Note that a singularity $\chi^{-1}\to 0$ is determined by the tendency of the correlation radii to grow to infinity with a diverging $\int h(r)d\mathbf{r}$. In Fig. 1 one immediately sees that the three approximations present SRBPs with finite values of the inverse compressibility, and complex solutions (dotted curves) emerge on the right side of the nonsolution boundary.

The situation in the liquid side of the phase diagram is similar for the HNC approximation for which the spinodal is again unattainable. One can see also that complex solutions appear now on the left side of the nonsolution boundary. As to the PY and MS approximations both have solutions up to the spinodal line, with an inverse heat capacity decreasing but remaining well away from zero in the vicinity of the spinodal. This is interesting, since the structure of Eqs. (18) and (19) would seem to suggest that a divergence in the OZ equation would induce a similar divergence in the equation for the temperature derivatives. The fact that this is not the case indicates that the zero in the denominator of Eq. (19) is counteracted by a corresponding zero in the numerator. These features are again fully consistent with the behavior of the correlation functions presented in Fig. 3. Incidentally, both these equations have nearby singularities well separated

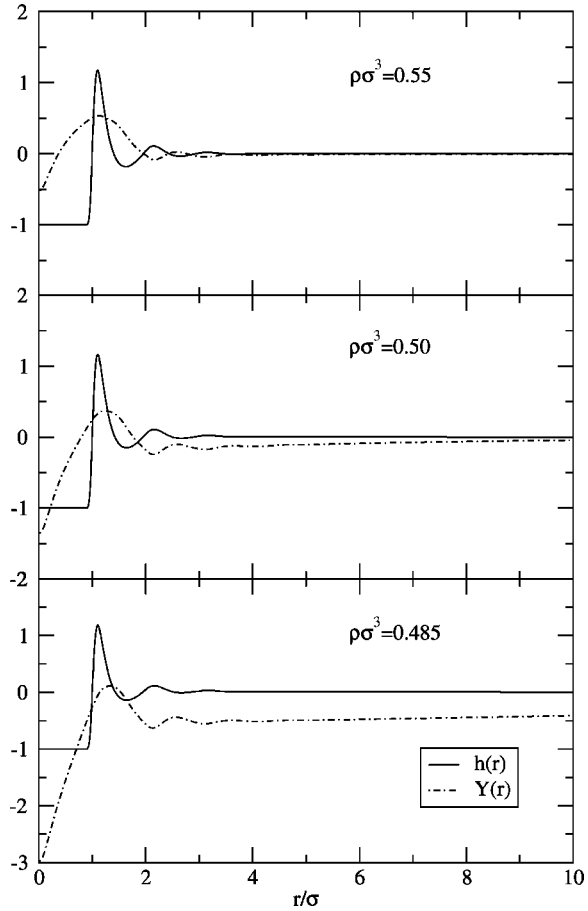

FIG. 3. Same as Fig. 2 for densities on the liquid side of the phase diagram.

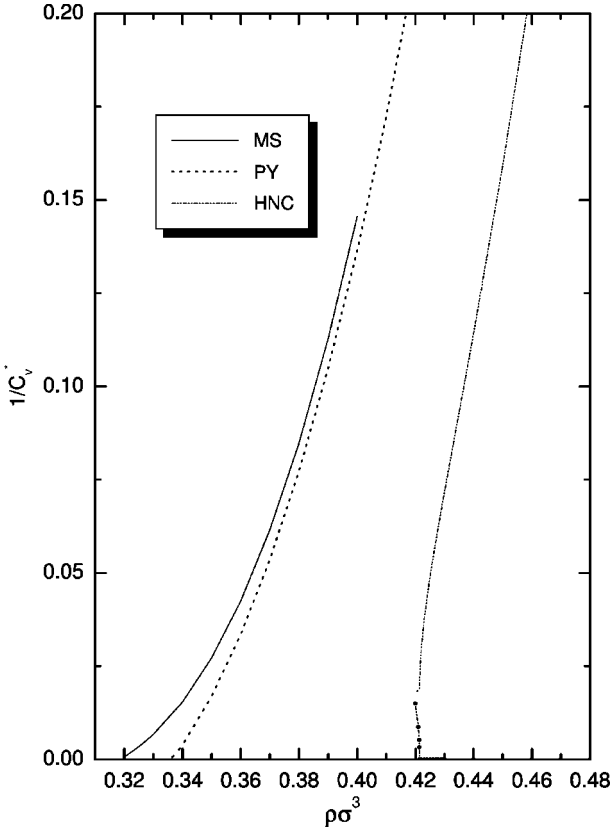

FIG. 4. Real and imaginary components of the inverse of the isothermal compressibility at temperature $T^*=1.3$ for various integral equation approximations in the neighborhood of the liquid–vapor transition on the liquid side of the phase diagram. Labels as in Fig. 1.

from the HNC nonsolution points. For the PY equation the transition from this type of behavior to the one found on the vapor side of the phase diagram is expected to happen right at the critical point,[7] and it is very likely that this will also be the case of the MS approximation.

Note also that, as found in Ref. 3, the isothermal compressibility of the HNC tends to diverge on the liquid side of the phase diagram as the temperature is lowered. At the same time, if the temperature is raised, the complex solutions are more easily attained and the nonsolution curve is hit at larger values of the inverse compressibility. This is illustrated in Fig. 4 for $T^*=1.3$. At even higher temperatures it is possible to cross the nonsolution region joining the vapor and the liquid side of the phase diagram[3] with a continuous complex solution. Finally, a few words regarding the complex solutions of the PY and MS equations on the liquid side of the phase diagram. Following the strategy explained in the previous section, it is possible to obtain converged complex solutions when the perturbing parameter $\epsilon=0.001$. However, from these initial solutions it is not possible to solve the equations for $\epsilon=0$. Moreover, the numerical solution of the PY and MS (and the HNC at low temperatures) easily crosses the nonsolution boundary, rendering spurious solutions with negative compressibility. These are actually solutions that present a pole for finite nonzero k in Eqs. (18) and (19) which, when dealt with semianalytically, produces correlations with long-ranged oscillatory behavior, a likely signature of the presence of inhomogeneities.[6]

Obviously, the fact that on the liquid side of the phase diagram compressibility diverges, whereas the heat capacity remains finite reflects the lack of thermodynamic consistency of the approximations. On the other hand, the situation on the vapor side of the phase diagram is somewhat less clear. All three approximations used here account properly for the effects of pairing and reproduce the exact second virial coefficient, and thus are correct up to $O(\rho^2)$. This is specially true as one lowers the temperature, since then the equilibrium densities substantially decrease. If we now think of what happens in a physical system when the density is increased along an isotherm on the vapor side of the phase diagram, it is obvious that once the binodal is crossed we have a supersaturated vapor, by which our low-density homogeneous system starts nucleating, i.e., particles begin to aggregate in clusters and homogeneity is lost. In our opinion, the onset of complex solutions is the way the equations have to tell us that our original homogeneous system (for which they are not only valid, but also almost exact at low densities) no longer exists. This is actually the idea that was exploited to successfully apply the multidensity integral-equation formalism in the HNC approximation to the restricted primitive model of electrolytes at low density.[16] This is an extreme situation in which the HNC equation does not even reach the binodal curve and where clustering is the leading physical feature. Only a proper account of clustering effects can cure the deficiencies of the HNC and related approximations in the low-density low-temperature regime.

ACKNOWLEDGMENTS

E.L. acknowledges financial support of the Dirección General de Investigación Científica y Técnica under Grant No. FIS2004-02954-C03-01. This work has been carried out under the auspices of the exchange agreement between the Consejo Superior de Investigaciones Científicas and the Russian Academy of Sciencies, which supported the exchange visits of E.L. and G.S. in the past two years.

[1]E. Lomba and G. N. Sarkisov, Russ. J. Phys. Chem. **79**, 38 (2005).
[2]G. Sarkisov, J. Chem. Phys. **114**, 9496 (2001).
[3]E. Lomba and J. L. López-Martín, J. Stat. Phys. **80**, 825 (1995).
[4]L. Belloni, J. Chem. Phys. **98**, 8080 (1993).
[5]J. S. Høye, E. Lomba, and G. Stell, Mol. Phys. **75**, 1217 (1992).
[6]L. J. Root and R. Lovett, J. Chem. Phys. **85**, 8390 (1991).
[7]P. T. Cummings and G. Stell, J. Chem. Phys. **78**, 1917 (1983).
[8]P. T. Cummings and P. A. Monson, J. Chem. Phys. **82**, 4303 (1985).
[9]G. E. Uhlenbeck and G. W. Ford, *Lectures in Statistical Mechanics* (American Mathematical Society, Providence, 1963).
[10]G. A. Martynov and G. N. Sarkisov, Mol. Phys. **49**, 1495 (1983).
[11]D. M. Duh and A. D. J. Haymet, J. Chem. Phys. **103**, 2625 (1995); D. M. Duh and D. Henderson, *ibid.* **104**, 6742 (1996).
[12]J. D. Weeks, D. Chandler, and H. C. Andersen, J. Chem. Phys. **54**, 5237 (1971).
[13]K. Ng, J. Chem. Phys. **61**, 2680 (1974).
[14]S. Labik, A. Malievsky, and P. Vonka, Mol. Phys. **56**, 709 (1985).
[15]G. N. Sarkisov, J. Chem. Phys. **119**, 373 (2003).
[16]Y. V. Kalyuzhnyi, V. Vlachy, M. F. Holovko, and G. Stell, J. Chem. Phys. **102**, 5770 (1995).